JOURNAL OF GEOPHYSICAL RESEARCH, VOL. 114, D13204, doi:10.1029/2008JD011574, 2009

Subarctic atmospheric aerosol composition: 2. Hygroscopic growth properties

Hanna Herich,[1] Lukas Kammermann,[2] Beth Friedman,[3,4] Deborah S. Gross,[4] Ernest Weingartner,[2] Ulrike Lohmann,[1] Peter Spichtinger,[1] Martin Gysel,[2] Urs Baltensperger,[2] and Daniel J. Cziczo[1,5]

Received 3 December 2008; revised 26 March 2009; accepted 30 April 2009; published 10 July 2009.

[1] Subarctic aerosols were sampled during July 2007 at the Abisko Scientific Research Station Stordalen site in northern Sweden with an instrument setup consisting of a custom-built Hygroscopicity Tandem Differential Mobility Analyzer (HTDMA) connected in series to a single particle mass spectrometer. Aerosol chemical composition in the form of bipolar single particle mass spectra was determined as a function of hygroscopic growth both in situ and in real time. The HTDMA was deployed at a relative humidity of 82%, and particles with a dry mobility diameter of 260 nm were selected. Aerosols from two distinct air masses were analyzed during the sampling period. Sea salt aerosols were found to be the dominant particle group with the highest hygroscopicity. High intensities of sodium and related peaks in the mass spectra were identified as exclusive markers for large hygroscopic growth. Particles from biomass combustion were found to be the least hygroscopic aerosol category. Species normally considered soluble (e.g., sulfates and nitrates) were found in particles ranging from high to low hygroscopicity. Furthermore, the signal intensities of the peaks related to these species did not correlate with hygroscopicity.

Citation: Herich, H., L. Kammermann, B. Friedman, D. S. Gross, E. Weingartner, U. Lohmann, P. Spichtinger, M. Gysel, U. Baltensperger, and D. J. Cziczo (2009), Subarctic atmospheric aerosol composition: 2. Hygroscopic growth properties, *J. Geophys. Res.*, *114*, D13204, doi:10.1029/2008JD011574.

1. Introduction

[2] Aerosol particles have a significant impact on atmospheric processes and are important when considering climate forcing [*IPCC*, 2007]. They absorb and scatter radiation (the ''direct aerosol effect'') [*McCormick and Ludwig*, 1967; *Charlson and Pilat*, 1969] but can also affect climate by acting as cloud condensation nuclei (CCN) and thus influence cloud albedo, persistence, and other cloud properties (the ''indirect aerosol effect'') [*Twomey*, 1977; *Rosenfeld and Lensky*, 1998; *Lohmann and Feichter*, 2005]. Both aerosol effects are linked to the interaction between aerosol particles and water vapor in the atmosphere. Whether an aerosol particle has the ability to take up water and ultimately activate as a CCN is determined both by its size [*Dusek et al.*, 2006] and its chemical composition [*Baltensperger et al.*, 2002; *Hegg et al.*, 2006].

[3] In addition to climate, there are other reasons why the water content of aerosol particles is of interest. For example, it has been shown that heterogeneous chemistry, such as the N_2O_5 hydrolysis reaction, only takes place effectively on the surface of aqueous aerosol particles. This reaction can remove NO_x from the atmosphere and leads to the formation of longer-lived HNO_3. Reaction rates for several aqueous aerosol surfaces have been determined in laboratory studies [e.g., *Mozurkewich and Calvert*, 1988; *Hu and Abbatt*, 1997].

[4] Aerosol optical properties correlate strongly with particle water content and thus depend on the ambient relative humidity (RH). In addition to direct aerosol effects, these properties determine local air quality and visibility [e.g., *Malm et al.*, 2003; *Franke et al.*, 2003]. Aerosol effects are especially important for polluted regions with high aerosol loadings, such as those with significant anthropogenic sources [e.g., *Satheesh and Ramanathan*, 2000; *Yu et al.*, 2006]. For remote regions like the Arctic the situation is more difficult to constrain. There are several known ways that aerosols in polar regions can perturb the radiation balance of the Earth-atmosphere system. A summary of the surface forcing and corresponding temperature response is given by *Quinn et al.* [2008]. These issues are of contemporary interest since one of the objectives of most recent International Polar Year (A Framework for the International Polar Year 2007–2008 produced by the ICSU IPY 2007–2008 Planning Group, 2004, International Council for Science, available at http://www.ipy.org) is to con-

[1]Institute for Atmospheric and Climate Science, ETH Zurich, Zurich, Switzerland.
[2]Laboratory of Atmospheric Chemistry, Paul Scherrer Institut, Villigen, Switzerland.
[3]Department of Atmospheric Sciences, University of Washington, Seattle, Washington, USA.
[4]Department of Chemistry, Carleton College, Northfield, Minnesota, USA.
[5]Now at Atmospheric Science and Global Change, Pacific Northwest National Laboratory, Richland, Washington, USA.

0148-0227/09/2008JD011574$09.00

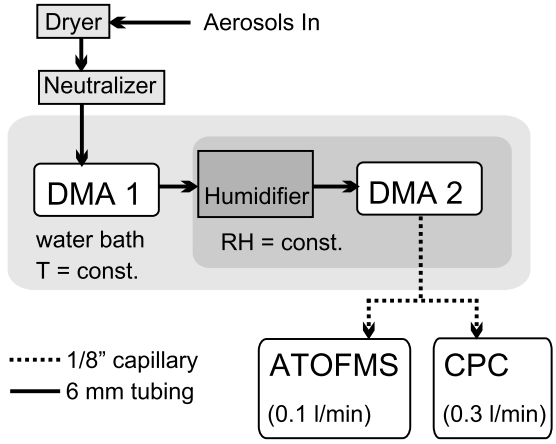

Figure 1. Experimental setup. In DMA1 of the HTDMA, incoming aerosols are size segregated. They are then humidified. The size distribution after humidification is monitored with scans from DMA2 and a condensation particle counter (CPC). In parallel, single particle mass spectra of the exiting particles are determined with an ATOFMS.

duct research studies of atmospheric processes in polar regions.

[5] Past measurements in Arctic regions have concentrated on the Arctic Haze phenomenon, which occurs during late winter and spring [*Iversen and Joranger*, 1985; *Klonecki et al.*, 2003], and measurements of Arctic and subarctic nucleation events [*Kulmala et al.*, 2001]. A smaller number of studies [*Hämeri et al.*, 2001; *Ehn et al.*, 2007] investigated hygroscopic properties of aerosol particles at high latitudes and compared results to impactor samples and gaseous sulfuric acid concentrations. These boreal forest particle studies concentrated on fine nucleation and Aitken mode particles. Aerosol properties, specifically hygroscopic growth as a function of chemical composition at the single particle level, remains essentially unknown for clean summer conditions for Arctic and subarctic regions.

[6] Several studies outside the Arctic have been performed which relate the hygroscopic growth of aerosol particles to their chemical composition. This has been done in the laboratory for pure chemical compounds and compounds in known mixing ratios [e.g., *Kreidenweis et al.*, 2005; *Koehler et al.*, 2005; *Svenningsson et al.*, 2006]. For ambient aerosols data remains much more limited. *Pitchford and McMurry* [1994] used X-ray fluorescence and ion chromatography and *McMurry et al.* [1996] used electron microscopy (EM) to determine the chemical composition of particles with known hygroscopicity, but in neither of these cases could it be obtained in real time. *Buzorius et al.* [2002] and *Zelenyuk et al.* [2008] deployed a Single Particle Laser Ablation Time-of-Fight Mass Spectrometer (SPLAT-MS) to determine the aerosol chemical composition, but these studies concentrated mainly on laboratory data.

[7] Recently *Herich et al.* [2008], hereafter H08, investigated chemical composition as a function of hygroscopic growth for atmospheric aerosols and showed that it is more complex than has so far been assumed. H08 found that species normally considered to be soluble (sulfates and nitrates) were also present in nonhygroscopic aerosols at both urban and remote field sites. The setup used by H08 consisted of a Hygroscopicity Tandem Differential Mobility Analyzer (HTDMA) [*Liu et al.*, 1978] connected in series with a single particle mass spectrometer. Specifically, an Aerosol Time-of-Flight Mass Spectrometer (ATOFMS) [*Gard et al.*, 1997], commercially available from TSI (Model 3800, TSI Inc., Minnesota), was used.

[8] HTDMAs are used to determine the water uptake of aerosol particles in terms of their hygroscopic growth factor. The growth factor (GF) is a quantity describing the water uptake of an aerosol particle at a certain RH, defined as

$$\mathrm{GF(RH)} = D_{\mathrm{RH}}/D_0, \tag{1}$$

where D_{RH} is the particle diameter for a certain RH, D_0 is the dry size of the particle, theoretically the diameter at 0% RH. By analyzing the HTDMA output with an ATOFMS, single particle chemical composition can be obtained as a function of the GF. Hence, this setup aims to elucidate the link between chemical composition, mixing state, and hygroscopic properties. In this work the same setup as used by H08 was deployed during a field campaign at the Abisko Research Station Stordalen field site operated by the Royal Swedish Academy of Sciences. Stordalen is located in northern Sweden and lies about 200 km above the Arctic Circle. The field campaign was conducted in support of the IPY and is fully described by *Friedman et al.* [2009]. Of the multiple objectives one was characterization of Arctic aerosol hygroscopicity as a function of composition. Owing to multiple scientific goals the connected HTDMA/ATOFMS setup was deployed for only parts of the 3-week study.

2. Experimental Procedure

2.1. Measurement Setup

[9] The experimental setup used during these studies, shown in Figure 1, has been described in more detail by H08. Briefly, aerosols are initially dried in a Nafion dryer to ~20% RH before they are sent to a krypton-85 neutralizer. Singly charged particles enter a HTDMA system consisting of two differential mobility analyzers (DMAs) separated by a humidification section. Possibly interferences from doubly charged particles are of minor importance because the selected dry size is on the tailing edge of the number size distribution. The DMAs are custom-built by the Paul Scherrer Institute and are based on the TSI 3071 column. DMA1 selects a narrow size range out of the dried polydisperse aerosol distribution. The monodisperse output, defined as dry mobility diameter D_0, is then humidified. Inside DMA2 the humidity is kept constant and is monitored and controlled with a dew point sensor. The entire HTDMA setup is placed in a cooled water bath with a temperature typically 5°C below the laboratory or field site. Specific details on the design of this HTDMA is given by *Weingartner et al.* [2002]. The humidified aerosol passes DMA2 and is split to a condensation particle counter (CPC) and an ATOFMS. The ATOFMS operates with a flow rate of 0.1 L/min and the CPC 1.0 L/min (TSI, Model 3010). The latter flow is diluted with 0.7 L/min particle free air to ensure a stable flow to the ATOFMS and to maintain suitable flow ratios in the DMAs of the HTDMA. To

minimize delay times (~10 s) capillaries are used for aerosol transport to the CPC and the ATOFMS. DMA2 is either operated in a scanning mode to observe particle size changes due to humidification or is set stepwise to specific sizes in order to sample particles with different GFs for longer time periods. During these experiments, a 6-min scan was performed approximately once per hour while the remainder of the time DMA2 was set to transmit particles with different GFs stepwise. In this manner aerosol concentration after the HTDMA as a function of GF was determined with the CPC and the chemical composition of single particles was simultaneously determined with the ATOFMS. The raw measurement distribution functions (MDFs) recorded after the HTDMA while operating in scanning mode were inverted with the TDMAinv algorithm [*Gysel et al.*, 2009] in order to retrieve the growth factor probability density functions (GF-PDF).

[10] The ATOFMS has been fully described by *Gard et al.* [1997]. Briefly, particles are focused with an aerodynamic lens [*Liu et al.*, 1995a] and are then accelerated by a nozzle such that their velocity is a function of their aerodynamic diameter. After two stages of differential pumping, the particles pass through the beams of two neodymium-doped yttrium aluminum garnet (Nd:YAG) sizing lasers (λ = 532 nm) which are set apart from each other at a known distance. The scattering signals of each laser is detected with a separate photomultiplier and this allows for a calculation of the particle's flight velocity. Particles then pass into the mass spectrometer region where they are desorbed and ionized by a fourth harmonic Nd:YAG, (λ = 266 nm) laser which is triggered on the basis of the calculated flight velocity. Typically ~20% of particles which transit both sizing lasers are struck by the desorption and ionization laser. Ions are generated and accelerated into the two time-of-flight mass spectrometers according to their polarity. Positive and negative mass spectra are simultaneously obtained in real time at the single particle level.

[11] It is important to note that the ATOFMS is a qualitative instrument. The peak heights, measured as a quantity of ions, in the bipolar mass spectra result from ions generated in the desorption and ionization step and the ion transmission efficiency through the mass spectrometer. Several processes can impact ion generation including the distribution of components through the aerosol (i.e., surface or interior) and the ionization efficiency of the specific material [*Gross et al.*, 2000; *Wenzel et al.*, 2003; *Murphy*, 2007]. Mass spectral peak heights therefore cannot be directly related to the component quantities without extensive laboratory determination of these effects [*Cziczo et al.*, 2001; *Dessiaterik et al.*, 2003]. Furthermore, it is possible that there are biases in the detection efficiency of particles with different components. However, H08 showed that for typical internally mixed atmospheric aerosol particles the hit rate with the ATOFMS, defined as the ratio of particles which produced a mass spectrum over total detected particles, did not vary significantly as a function of GF.

[12] The size range of aerosols that can be analyzed with the ATOFMS is limited by the detection/sizing laser signals and the aerodynamic lens. Light scattering intensity gives a lower size limit of approximately 150 nm (i.e., smaller particles scatter insufficient light to create a detectable signal at the photomultipliers) although transmission begins to fall off below 300 nm with the aerodynamic lens system used here. Aerodynamic focusing falls off above ~600 nm [*Liu et al.*, 1995a, 1995b] with no particles larger than 2 μm observed during these studies. Particles with a size of 260 nm were found to be the smallest with sufficient light scattering intensity for detection, high aerodynamic transmission efficiency, and high hit rate with the desorption and ionization laser. This size is within the range where it can be assumed that particles are fully desorbed during the desorption/ionization process [*Weiss et al.*, 1997]. Particles of 260 nm diameter were therefore selected as the incoming dry aerosol size (i.e., D_0 in equation (1)) in the experiments described here. This, at a RH of 82%, was also the maximum size before arcing in DMA2 occurred at the highest voltages required for the largest growth factors. In typical ambient aerosols, 260-nm particles generally belong to a portion of the distribution above the number maximum, often close to the mode of the volume distribution [*Weingartner et al.*, 1999]. This was also the case during the Stordalen measurements [*Friedman et al.*, 2009].

[13] A humidity of 82% is relatively low compared to other HTDMA experiments and is not far above the deliquescence RH (DRH) of some inorganic salts; it is at or slightly below the DRH of some pure organic compounds [*Seinfeld and Pandis*, 2006]. It is, however, unlikely that this impacts the ambient particles studied here. It has been observed that the highest DRH for aerosol particles consisting of a mixture of different compounds with different DRHs is lower than the lowest DRH of the individual compounds. With an increasing number of soluble compounds the growth curve does not exhibit a distinct deliquescence point but instead a continuous water uptake [*Marcolli et al.*, 2004]. Aged atmospheric particles are largely internally mixed and consist of different inorganic and organic compounds [*Murphy et al.*, 2006]. The efflorescence RH (ERH) also shifts to a lower value with increasing compound number in the mixture, ultimately leading to the particle exhibiting no efflorescence. Because of this, typical aged, internally mixed atmospheric particles will often not dry completely at low RHs, instead containing a small residual amount of water. Indeed, previous HTDMA studies of atmospheric aerosols show that indications of a clear deliquescence signal were found in only a few cases (summarized by *Swietlicki et al.* [2008]). It is therefore assumed that 82% RH is above the range where hysteresis behavior occurs. Despite this generality it has been shown that some pure organic compounds may require a longer time than commonly used for HTDMAs to reach equilibrium with water vapor [*Chan and Chan*, 2005; *Sjogren et al.*, 2007]. The residence time between the two DMAs for the setup described here is approximately 20s, which is higher than typically used for HTDMAs.

2.2. Sampling Site and Measurements

[14] Measurements were performed at the Abisko Scientific Research Station Stordalen field site (68°22′N 19°03′E), administered by the Royal Swedish Academy of Sciences, which is located 200 km north of the Arctic Circle and 385 m above sea level (msl). It is a reserve most often used for ecological studies [e.g., *Sonesson*, 1980; *Sohlenius and Boström*, 1999]. Stordalen is an Arctic mire and peat-

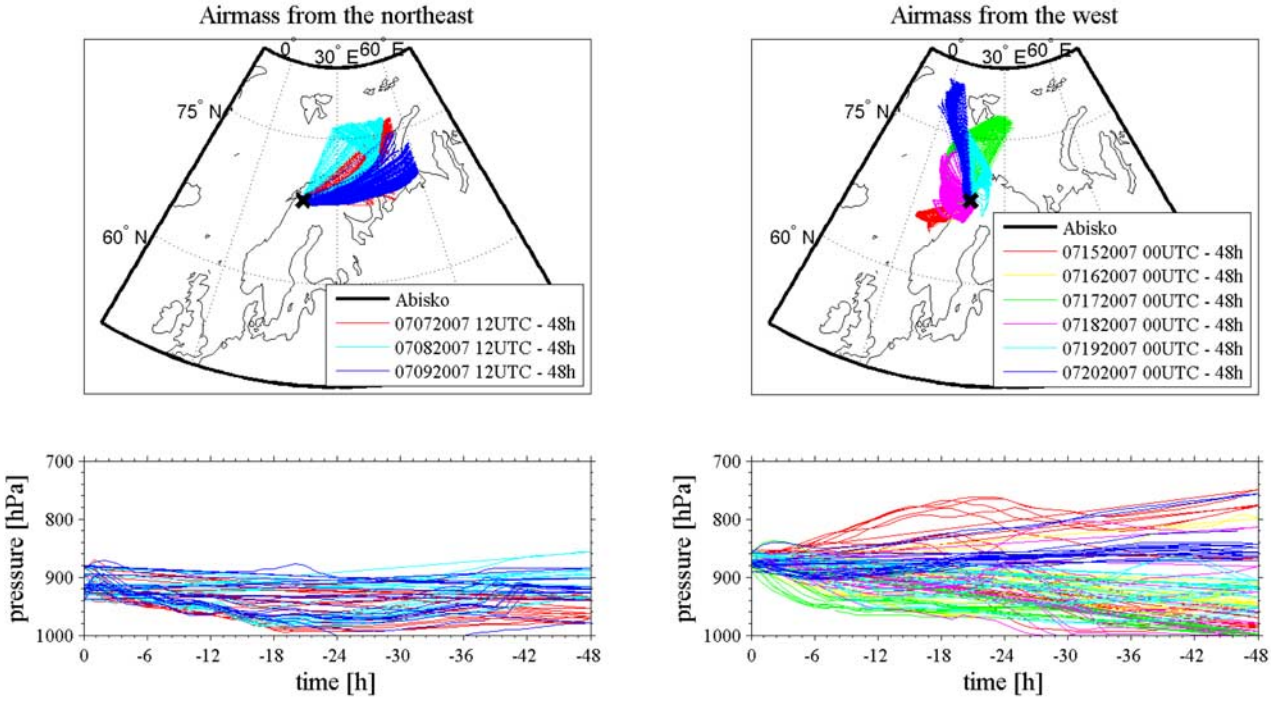

Figure 2. (top left) The 48-h back trajectories for Abisko for 7–9 July 2007 initialized in 24-h intervals. (bottom left) Vertical cross section of the trajectories. (top right) The 48-h back trajectories for Abisko for 15–20 July 2007 initialized in 24-h intervals. (bottom right) Vertical cross section of the trajectories. For clarity, only every tenth trajectory is shown in the vertical cross sections.

land area situated in a zone of discontinuous permafrost. The vegetation consists mainly of birch trees and boreal forest which are a source for aerosol nucleation events [*Svenningsson et al.*, 2008]. This remote area is located 1 km to the east of the only large road which connects Narvik and Kiruna (both ~90 km from Stordalen); the site is only accessible through a footpath or helicopter. About 1 km to the east of Stordalen lies Lake Torneträsk and 10 km to the west is the village of Abisko which has about 150 permanent inhabitants. The Abisko area has a railway connection; the railroad is frequently used by open freight trains shipping ore from Kiruna to Narvik and has to be considered as a local aerosol source. The large-scale topography of the region is, briefly, the following: The region east of Abisko, toward northern Finland, Russia and the Barents Sea, is relatively flat and below 500 msl. To the north, west and southwest the area borders the Scandinavian Mountains which have elevations on the order of 1000 to 2000 msl. Behind the mountain range lies the coast and Norwegian Sea. The entire area is sparsely populated and the closest major pollutant sources are Nikel, Murmansk and Montshegorsk to the north/northeast. These contain nonferrous metal smelters and aluminum fabrication [*Hatakka et al.*, 2003]. Sources in the west are smelters and the metal production industry in northern Norway. More information is given by *Friedman et al.* [2009].

[15] Aerosol samples were taken from an isokinetic PM-10 inlet (URG, Model 2000–30DBQ) mounted on a measuring cabin situated on a small bank within the Stordalen mire site. Measurements were taken during July 2007. July, with an average temperature of +11°C, is the warmest month of the year in the region. Daylight is continuous during this period given the latitude. The HTDMA-ATOFMS setup was deployed during two portions of the study. A first data set was obtained from 7 to 9 July 2007 and a second from 14 to 20 July 2007. During both sampling periods, stable wind conditions dominated. In the first period, the air mass originated from the northeast (NE) while during the second period an air mass from the west (W) was sampled. A third air mass, from the south, was not sampled with the HTDMA-ATOFMS combination but is described by *Friedman et al.* [2009].

[16] For a detailed investigation of the air mass origin the Lagrangian trajectory model LAGRANTO [*Wernli and Davies*, 1997] was used. Meteorological analyses from the European Center for Medium-Range Weather Forecasts (ECMWF) were used as input for the model. The data are available for standardized times (0000, 0600, 1200, and 1800 UTC) on 91 model levels and are interpolated on a fixed Gaussian grid ($0.25° \times 0.25°$). The position of the air parcels is determined from the 3-D wind fields; however, for more detailed investigations (see section 3.2), the variables temperature, specific humidity and cloud liquid water mixing ratio are interpolated on the trajectories. The standard trajectories were calculated every day for 1200 and 0000 UTC arrival time at the field site. Trajectories are shown in Figure 2 for both air masses considered here. Trajectories for the remainder of the month are given by *Friedman et al.* [2009].

[17] At times other than these two sampling periods, and for other short time intervals during the study, the ATOFMS took mass spectra from the polydisperse background aerosol straight from the aerosol inlet. These data sets are designated as "background aerosol." The size range of the

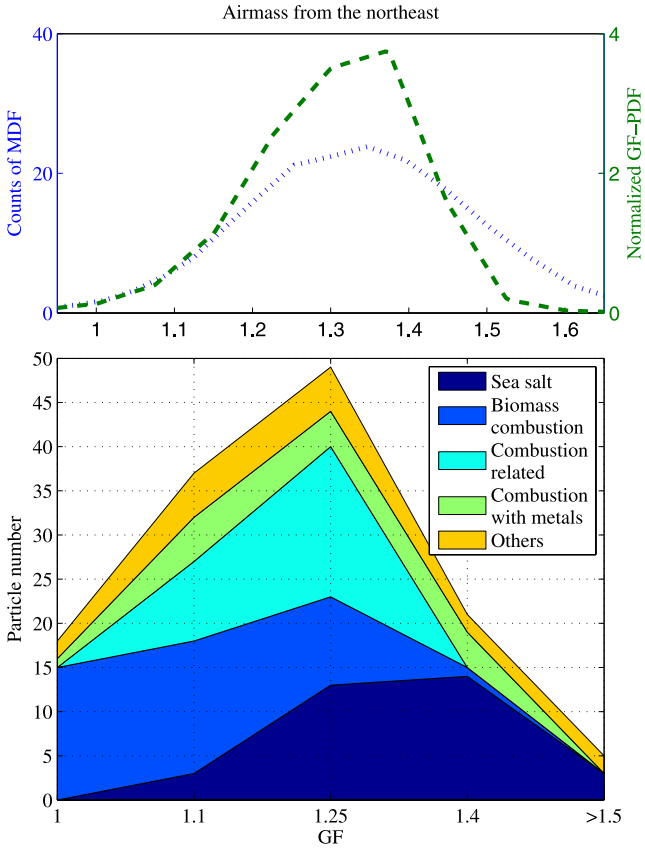

Figure 3. (top) Average of HTDMA scans for the air mass from the northeast with a measurement distribution function (MDF, left scale) and growth factor probability density function (GF-PDF, right scale). (bottom) Clustered particle compositions and their occurrence as a function of GF for the air mass from the northeast.

background aerosol mass distribution lies roughly between 0.25 and 2 μm and this is affected by the transmission of the ATOFMS inlet (see section 2.1). During the sampling period the number size distribution of the ambient aerosol was measured continuously with a scanning mobility particle sizer (SMPS) system. While there were often high particle number concentrations (up to 3000 cm^{-3} for the air mass from the NE and up to 7000 cm^{-3} for the air mass from the W) this was predominantly in the size range from 10 to 230 nm owing to nucleation events. The size range above 230 nm was largely unaffected by these events and the number concentrations in this range were comparatively low (100–300 cm^{-3} for air mass from the NE and 70–500 cm^{-3} for air mass from the W).

3. Results

3.1. Air Mass From the Northeast

[18] During the 7–9 July 2007 time period the GF-PDF for 260-nm particles from HTDMA scan data showed a single broad peak from GF = 1.0 to 1.6 with a maximum at approximately 1.35 (Figure 3, top). This range was divided into 5 bins because DMA2 transmitted particles with GFs 1.0, 1.11, 1.26, 1.39 and 1.47 stepwise to the ATOFMS; a few particles with intermediate GFs were also detected when DMA2 was periodically in scanning mode. In the subsequent analysis all particles were placed in one of the following GF center bins: 1.0, 1.1, 1.25, 1.4 and 1.5 and above. In total, 130 bipolar single particle mass spectra from the air mass from the NE were obtained. The mass spectra were initially sorted into four distinct particle categories: Sea salt, potassium-rich particles, carbon containing particles and a group of particles containing several metal and sulfate peaks plus common elemental or organic carbon related peaks.

[19] The first category, sea salt, includes particles which consisted of Na^+ (m/z = 23), K^+ (m/z = 39), often $^{35}Cl^-/^{37}Cl^-$ (m/z = −35/−37) or $Na_2{}^{35}Cl^-/Na_2{}^{37}Cl^-$ (m/z = 81/83), Na_2O^+ (m/z = 62), Na_2OH^+ or HNO_3^+ (m/z = 63), $Na_3SO_4^+$ (m/z = 165) and other sodium and chlorine related species. These peaks are all typical for ATOFMS sea salt mass spectra [*Gard et al.*, 1998; *Dall'Osto and Harrison*, 2006]. Further, NO_2^- (m/z = −46), NO_3^- (m/z = −62) and HSO_4^- (m/z = −97) peaks were often present as well as organic fragment peaks such as CN^-, $C_2H_2^-$ (m/z = −26) or CNO^- or $C_2H_2O^-$ (m/z = −42). Both peaks −26 and −42 have been previously observed in ATOFMS mass spectra; for example, *Holecek et al.* [2007] detected them in rainwater samples and assumed the peaks to be CN^-/CNO^- (i.e., organic nitrogen species). These peaks have also been observed in sea salt aerosols where they were used, among others, to identify organic material [e.g., *Middlebrook et al.*, 1998]. Sea salt is known to react with gas-phase HNO_3 which leads to a replacement of chlorine by nitrates. In our sea salt mass spectra we almost always observed NO_2^- and NO_3^- peaks although $Na_2{}^{35}Cl^-/Na_2{}^{37}Cl^-$ peaks were also often present. This implies that the aerosol had begun to undergo this reaction and we therefore described it as slightly aged sea salt.

[20] The second category was defined by potassium-rich particles. Besides potassium (K^+) these particles almost always contained sulfate and carbon peaks. Sulfate was defined by the masses SO_3^- (m/z = 80), HSO_3^- (m/z = 81), $^{97}HSO_4^-$ and $^{99}HSO_4^-$ (m/z = 97 and 99), $CH_3SO_4^-$ (m/z = 111), $HSO_4^-SO_3^-$ (m/z = 177) and $HSO_4H_2SO_4^-$ (m/z = 195) [*Murphy and Thomson*, 1997a]. Potassium not associated with sea salt and not in combination with mineral dust peaks can be identified as a biomass burning tracer [*Murphy and Thomson*, 1997b; *Silva et al.*, 1999; *Hudson et al.*, 2004]. Since temperatures in northern Scandinavia remain low even during the summer time, a likely source for the biomass particles is domestic heating. In addition, anthropogenic burning in combination with long-range transport might also be a possible source. The sulfate in the particles can be explained by aging processes (e.g., uptake and coagulation). This particle group is referred to as biomass combustion.

[21] A significant part of the remaining aerosol is defined as carbon-rich particles which likely originated from combustion. The mass spectra of these particles contained several elemental carbon (EC) peaks (C_n^+ and C_n^-, where n is an integer) in combination with organic carbon (OC). It is unlikely that the EC peaks resulted from biomass burning due to the absence of potassium. More likely, they originated from anthropogenic processes, for example, diesel soot. EC peaks may also be due to "charring" of organic material [*Schmid et al.*, 2001]. In almost all particle mass

spectra from the carbon-rich group, sulfate peaks were present. These particles are referred to as combustion related.

[22] The fourth group is defined as metal containing particles (i.e., containing one or more metal peaks). In almost all of these particles, sulfate peaks were present and the majority contained additional OC and/or EC peaks. Refractory materials included $^{107}Ag^+$ and $^{109}Ag^+$ (m/z = 107 and 109), Ba^+ (m/z = 138 and isotopes), Ca^+ (m/z = 40), Al^+ (m/z = 27), V^+ (m/z = 51) and Fe^+ (m/z = 56 and other isotopes). The metal containing particles were highly temporally correlated and these particles may have originated from industrial processes (e.g., from the Kola Peninsula area). These particles are referred to as combustion related with metals. The remaining 12% of particles could not be placed in these four main groups and will be referred to as "other."

[23] Figure 3 (bottom) shows the distribution of these particle categories as a function of their GF. All sea salt aerosols were found to have a GF of greater than 1.1 and particles with a GF of 1.4 and higher were nearly always sea salt. Potassium-rich particles, likely from biomass burning, were the major particle type in the nonhygroscopic regime; 83% of the particles with a GF of 1.0 were in this category. For particles with higher GFs, the fraction of potassium-rich aerosols decreased. Metal containing aerosols were found to have GFs in the range of 1.1 to 1.25. From the very distinct GF distribution of these particles they may have had a common source (i.e., distance and atmospheric lifetime from that source). Carbon-rich particles were found across the GF range.

[24] The data can be placed in hygroscopically different groups: first, sea salt particles, with an average GF of ~1.4, and non–sea salt particles, with a GF of 1.15–1.2. In addition, the non–sea salt particles can be divided into combustion particles with and without biomass residues where the biomass particles were found to be less hygroscopic. Studies in urban environments show aerosol groups with similar GFs as those for the less hygroscopic combustion particles [e.g., *Swietlicki et al.*, 2008]. It is assumed that these particles are mixtures of transported particles. The rather lower GF here indicates that the combustion aerosols may have been minimally aged which is supported by the trajectories which indicate that the aerosols may have originated in northern Finland or the Kola Peninsula. Hence, although Stordalen is a remote field site, a portion of the particles are similar to urban aerosols.

[25] Although the absolute peak areas do not provide quantitative information, relative quantities can be determined by comparing ratios of peak areas to the overall mass spectral area (i.e., relative peak area). This was demonstrated by *Middlebrook et al.* [2003] and *Murphy et al.* [2006], who compared data from single particle mass spectrometers with quantitative instruments such as particle-into-liquid samplers (PILS). Dependent on different ionization efficiencies and matrix effects, peak areas can be in very different orders of magnitudes for different chemical species. Toward this end, all peaks in each mass spectrum were normalized to a total relative area of 1. Peak ratios of certain compounds to the total area were then determined. For comparison, peak ratios for the background data set (762 particles) detected during the same sampling period were also determined. Figure 4 shows the correlation of various peak ratios with the GF of the particles. Grey dots indicate the ratios of the background aerosol sample for which GF is not measured. The peak ratios of the aerosols with known GF are overlaid, color coded by GF. Note that particles containing neither or only one of the compounds analyzed in each example have peak ratios of zero and therefore do not appear in Figure 4. The percentage of particles with known GF and for which both peaks appeared is represented in each plot.

[26] In Figure 4, the peak ratios of potassium, chlorine, nitrates and organics (from the fragment peaks CN^- or $C_2H_2^-$ and CNO^- or $C_2H_2O^-$) are shown as a function of the sodium, sulfate and EC peak ratios. Sodium, sulfates and nitrates are chosen since these compounds are hygroscopic and believed to be related to aerosol water uptake. In Figure 4a the sodium content, indicative of sea salt, distinguishes hygroscopic from nonhygroscopic particles. In total, 42% of the detected particles contained both sodium and potassium, common peaks in sea salt particles. The potassium peak area in sea salt particles is, on average, between 3 and 10%. In contrast, potassium accounts for 10 to 40% of the peak area in nonhygroscopic particles. Chlorine was common in sea salt particles where it accounts for 0.1–15% of the peak area. There are few nonhygroscopic particles with a chlorine peak (3%). In these particles the peak ratio is less than 0.1% and, at most, 7%. A total of 30% of the particles contained sodium and nitrates. For hygroscopic particles the peak ratio varies between 0.2 and 4%. In contrast the ratio is below 1% for nonhygroscopic particles. In total, 36% of the particles contained sodium and sulfates. Organics were common in sea salt particles and this is discussed in more detail in section 3.1.1.

[27] Figures 4b and 4c display the sulfate and EC correlations of the particles, respectively. These compounds are most abundant in non–sea salt particles and thus complement the first column data. In order to focus completely on the non–sea salt particles, only particles with a limited sodium content (below 0.05% ion ratio) are shown. Thus, the particles with a high GF and a high sodium content in Figure 4a (almost entirely sea salt) are excluded from Figures 4b and 4c.

[28] Figure 4b (first panel) correlates potassium with sulfate. This compound combination is common and occurs in 72% of the particles. There is a trend of increasing hygroscopicity with decreasing potassium content; particles with the lowest GFs often have potassium peak areas of 10% and greater. More hygroscopic particles often have sulfate peak areas of 3% and higher. Nevertheless, there are also particles with low GF and similar sulfate peak area which makes it impossible to relate the sulfate content and the GF. This finding is similar to the results of H08 who also found sulfate in both hygroscopic and nonhygroscopic aerosols. Figure 4b, second and third panels, relate chlorine and nitrates, respectively, as a function of sulfates; this compound combination occurs in only 17% and 22% of all particles, respectively. These are predominately the less hygroscopic ones. Sulfates and organics are common, appearing in 35% of the particles, and there is no clear correlation with the GF. Overall, the relative peak area of sulfates varies between 0.1% and 30%. There seems to be a

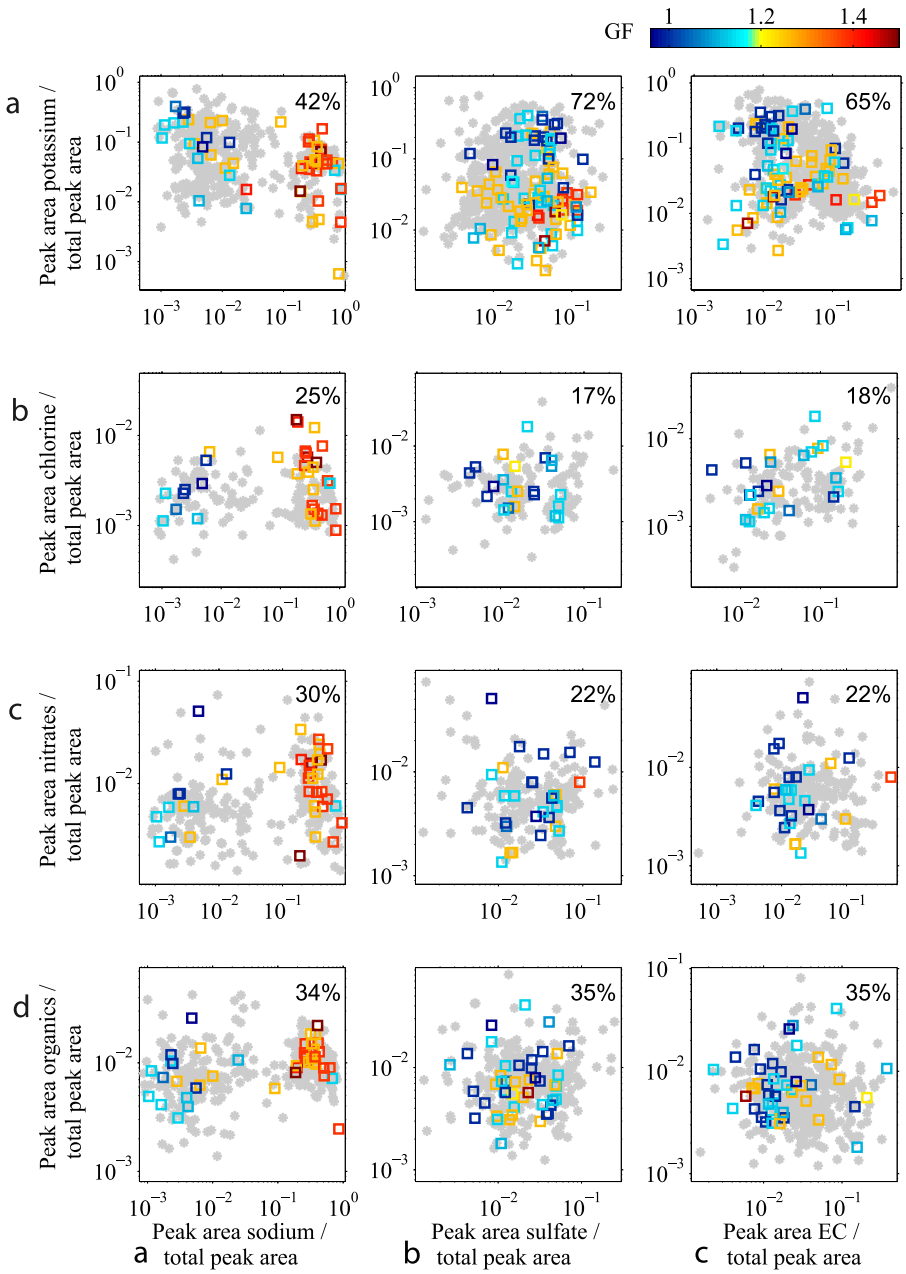

Figure 4. Correlation of different peak area ratios for aerosols from the air mass from the northeast. In each panel, peak ratios of two compounds are shown plotted against each other. Each dot represents a single particle. The gray dots indicate the ratios of an ambient sample (762 particles) taken during the same period. The peak ratios of the aerosols with known GF are overlaid, and the GF is color coded. Blue indicates a low GF, on the order of 1.0, whereas red indicates a GF of 1.4 and higher. Only single particles which contain both of the correlated compounds appear in the panels. The value in the upper right corner of each panel indicates the percentage of the total aerosols with GF information which meet these criteria. Owing to their sodium content, the focus of the left panels is sea salt particles. In the middle and right panels, sodium containing particles are excluded from the panels. This allows identification of the more hygroscopic, but non–sea salt, particles.

weak trend of decreasing GF with increasing organic peak ratio.

[29] Figure 4c presents combustion related particles with EC used as the abscissa. Potassium and EC peaks were present in 65% of the analyzed particles, which is a majority of the non–sea salt aerosol. The peak area of potassium varies between 0.1 and 40%. The particles with the smallest GFs, on the order of 1.0, have the highest potassium peak areas, on average above 10%; these are predominantly categorized as biomass burning particles (Figure 3). For EC, the peak areas vary between 0.1 and 60%. The average EC peak area for particles with a GF of 1.0 is ~1% while particles with a GF above 1.2 have on average peak areas of ~3%. This finding is contrary to what one might expect but

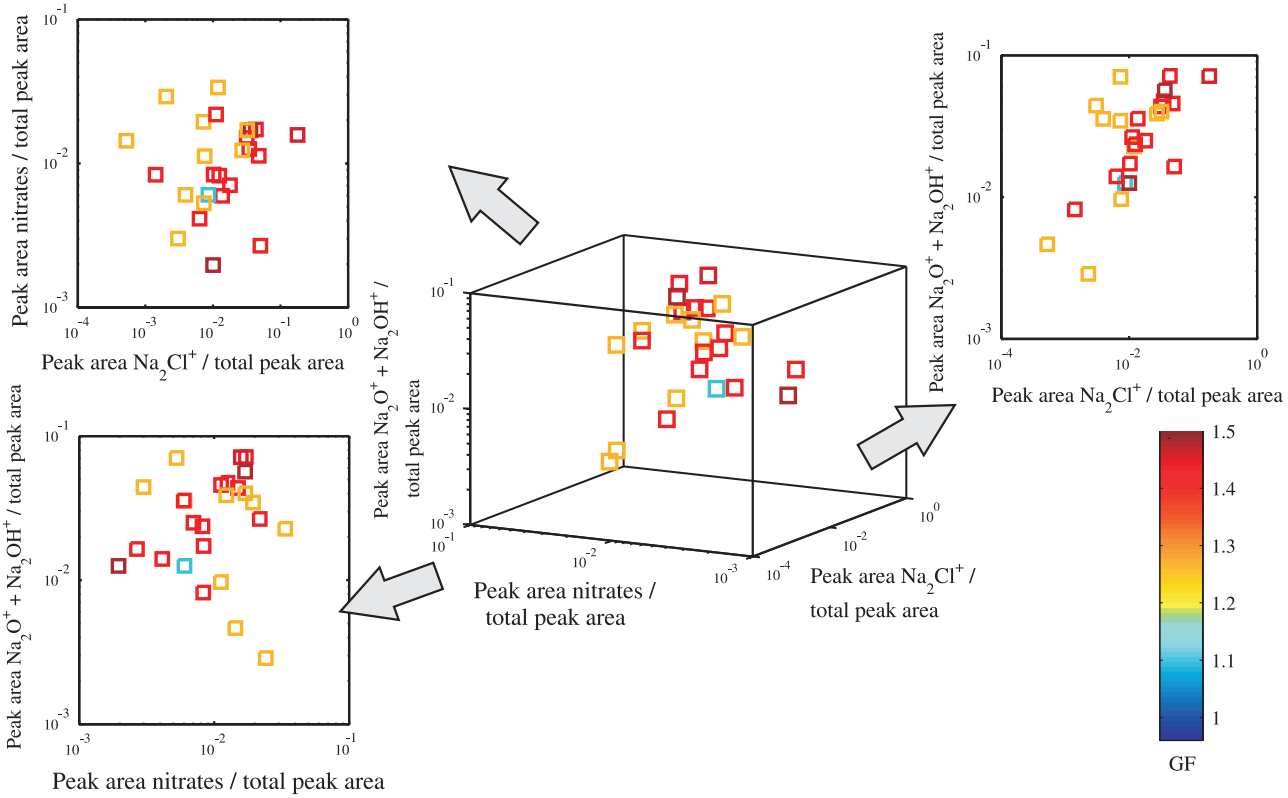

Figure 5. Correlation of different peak ratios for compounds related to sea salt aging. Sea salt particles were common in the air mass from the northeast. The middle image shows the peak area of nitrate species versus NaO^+ + $NaOH^+$ versus Na_2Cl^+ normalized to the total peak area for sampled particles which contained sodium (i.e., these particles are assumed to be of sea salt origin). The surrounding plots show the peak area correlations for each pair. The GF of each particle is color coded. Each dot represents a single particle.

it should not be interpreted as more EC-rich material being more hygroscopic. Instead, the slightly lower EC peak areas in GF = 1.0 particles are likely due to the increased relative signal of the potassium peak. For chlorine the peak area varies in the range of 0.5–2%, for nitrates in the range of 0.1–5%. The peak area of organics varies between 0.2 and 4%. There are fewer sea salt particles which also contain chlorine, nitrates, and organics plus EC peaks, only 18%, 22% and 35%, respectively. An interesting correlation is that particles with chlorine, nitrate and organics that are not sea salt particles are essentially all found in nonhygroscopic particles with GF < 1.2. Thus, these compounds were bimodally either found in very hygroscopic sea salt particles or in the nonhygroscopic non–sea salt aerosol.

3.1.1. Aging of Sea Salt

[30] For aerosols originating in the northeast, sea salt was the major source of the more hygroscopic particles. As previously mentioned, it has been shown that heterogeneous chemistry can take place in sea salt aerosols which then leads to a partitioning of gas-phase HNO_3 to solid- or aqueous-phase $NaNO_3$ [*Gard et al.*, 1998], according to reaction (1):

$$\text{(R1)}\quad HNO_3(g) + NaCl(s \text{ or } aq) \rightarrow NaNO_3(s \text{ or } aq) + HCl(g).$$

This process allows us to distinguish fresh and aged sea salt aerosols using mass spectral peak ratios. Typical ATOFMS mass spectra from fresh sea salt particles contain several chlorine related species, especially $^{35}Cl^-$ and $^{37}Cl^-$ and $Na_2^{35}Cl^-$ and $Na_2^{37}Cl^-$. Mass spectra of aged salt particles often contain peaks of Na_2O^+ and Na_2OH^+ as well as nitrates (NO_2^- and NO_3^-), the main fragments of $NaNO_3$ [e.g., *Dall'Osto and Harrison*, 2006]. Since our sea salt aerosol particles often contained both chlorine and nitrate fragments, we describe them as slightly aged.

[31] In Figure 5, correlations of the peaks of different sea salt related species are presented. This is analogous to Figure 4 but with a focus on whether the reacting and aging of the sea salt has an influence on the GF. From reaction (1) one expects an anticorrelation of the peak area from $Na_2^{35}Cl^-$ and $Na_2^{37}Cl^-$ with those of the nitrates species. Since Na_2OH^+ and Na_2O^+ are known to be markers for aged sea salt aerosols, they are expected to correlate with nitrates. In Figure 5 (top left) it can be observed that there is a slight correlation between the $Na_2^{35}Cl^-$ and $Na_2^{37}Cl^-$ and the nitrate content in the particles according to their GF. Most particles in which the relative peak area of $Na_2^{35}Cl^-$ and $Na_2^{37}Cl^-$ remains below ~1% have GFs of ~1.25. On the other hand, particles with a relative peak area of $Na_2^{35}Cl^-$ and $Na_2^{37}Cl^-$ above 1% have GFs of 1.4 and higher. In addition, mass spectra of particles where the peak area of $Na_2^{35}Cl^-$ and $Na_2^{37}Cl^-$ is low exhibit a slightly higher peak area of nitrates (above 1%). While the sample size is small,

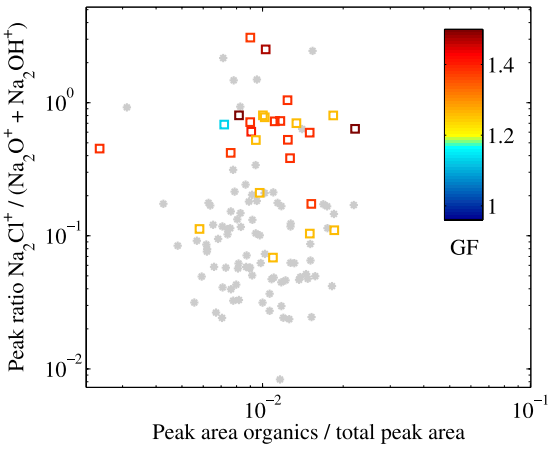

Figure 6. Correlation of Na_2Cl^+ to Na_2O^+ + Na_2OH^+ for particles which contained sodium (i.e., particles assumed to be of sea salt origin) for the air mass from the northeast. The gray dots indicate the ratios for ambient particles taken during the same sampling period. Peak areas of color-coded GF are overlaid. See text for further details.

the results do show a trend that aged sea salt aerosols are less hygroscopic than fresh ones.

3.1.2. Organics in Sea Salt Particles

[32] It is known that marine aerosols can contain large amounts of organic material [*Cavalli et al.*, 2004; *Middlebrook et al.*, 1998; *O'Dowd et al.*, 2004]. This is due to the formation process where organics on the surface layer is aerosolized via bubble bursting [*Blanchard*, 1983]. This organic enhancement mechanism is also thought to take place in the Arctic [*Leck and Bigg*, 1999]. Gas-phase organic species or secondary organic aerosols (SOA) can also be taken up or coagulate with preexisting sea salt aerosols, respectively. In northern Scandinavia, volatile organic compounds (VOCs) emitted from the boreal forest are known to contribute to gas-to-particle formation [*O'Dowd et al.*, 2002].

[33] The organic content of sea salt aerosols is of significant interest because this particle type is the most common over the oceans and is an important scatterer of shortwave radiation [*Schwartz*, 1996]. Soluble organics are known to change the water uptake of sea salt aerosols [*Saxena et al.*, 1995; *Ming and Russell*, 2001] which, in turn, has an influence on the refractive index of the particle and can lead to a reduction of scattering [*Randles et al.*, 2004]. In addition, organics can decrease or, as a limit prevent, CCN activity [e.g., *Leck et al.*, 2002] where organics that reduce the surface tension may increase CCN activity [e.g., *Lohmann and Leck*, 2005; *Feingold and Chuang*, 2002].

[34] The sea salt aerosol mass spectra acquired here contained peaks identified as fragments of organic material. Specifically, peaks −26 and −42 were common. Figure 4a (last panel) illustrates the variation of peak areas of these two organic marker with sea salt indicators. The left side of the panel is the organic compound peak ratio as a function of the sodium peak ratio. In the particles with a high sodium content the relative peak area of organics lies between ∼0.7–2%. In comparison, the relative area of organic peaks in particles with a low sodium content (i.e., non–sea salt particles) varies within a much larger range, between ∼0.2–4%.

[35] Figure 6 illustrates how the area of these two organic peaks varies as a function of the peak ratio Na_2Cl^+ to Na_2OH^+ and Na_2O^+ and the GF. As previously described, this peak ratio is related to the age of the sea salt aerosol. This peak ratio is larger, on average, for more hygroscopic particles. The peak area of the organics is similar, ∼1%, for all particles and there is little variation with GF or Na_2Cl^+ peak area. This suggests that fresh to aged sea salt aerosol has little difference in organic content and this lack of variation also suggests that the organics may be a primary constituent of these aerosols instead of accumulating with time and transport. The important caveats are that this is a small data set from one location and during a single season.

[36] A recent study by *Facchini et al.* [2008] found organics accounting for ∼50–90% of the mass of similar size sea salt particles to those studied here and that the organic content adversely affected hygroscopicity. That study was conducted in the North Atlantic during periods of phytoplankton bloom and used an artificial method for aerosol generation. These results are not consistent with what was found in this study in that organic content was not observed to correlate with hygroscopicity of sea salt particles. It needs to be considered that organic content of sea salt aerosols depends strongly on the location, season, and other factors (e.g., phytoplankton blooms) and that neither study can be taken as globally representative.

3.2. Air Mass From the West

[37] During the 14–20 July time period the air mass originated from the west to northwest of Abisko (i.e., the Norwegian Sea). These air masses passed the Scandinavian Mountain region before reaching Stordalen. The resulting uplift is apparent in the back trajectories and it can therefore be assumed that a large amount of the aerosol was wet deposited and/or scavenged before reaching Stordalen. This hypothesis is corroborated by a more detailed investigation of the 72-h back trajectories starting on 15 July 2007 at 0000 UTC in the region 18.5°E–19.0°E, 68.0°N–68.5°N near the ground (p = 920–850 hPa) as shown in Figure 7. The back trajectories are color coded by their cloud water mixing ratio, which can be interpreted as a cloud proxy. Important for this investigation is the fact that at least during the ascent of the air parcels cloud water mixing ratio is increasing, indicating the formation of a cloud in this area. Thus, it is very likely that air parcels experience the formation and/or presence of a cloud during their evolution. Hence, sea salt aerosols, as very good CCN, probably formed rain droplets and were efficiently removed via precipitation from the ambient aerosols; as described in the following paragraphs, despite the maritime origin of the air mass, sea salt was not common. As further evidence for this hypothesis, precipitation data from the Swedish Meteorological and Hydrological Institute for the measurement site Katterjakk, located 35 km west of Abisko, shows that precipitation took place during the measurement period in the mountain areas.

[38] From 14 to 20 July 2007, 260-nm particles had a GF-PDF distributed in a single mode from 1.0 to 1.55 with a mode of ∼1.35 (Figure 8, top). DMA2 of the HTDMA was set to stepwise transmit particles with GF 1.0, 1.1, 1.2, 1.3,

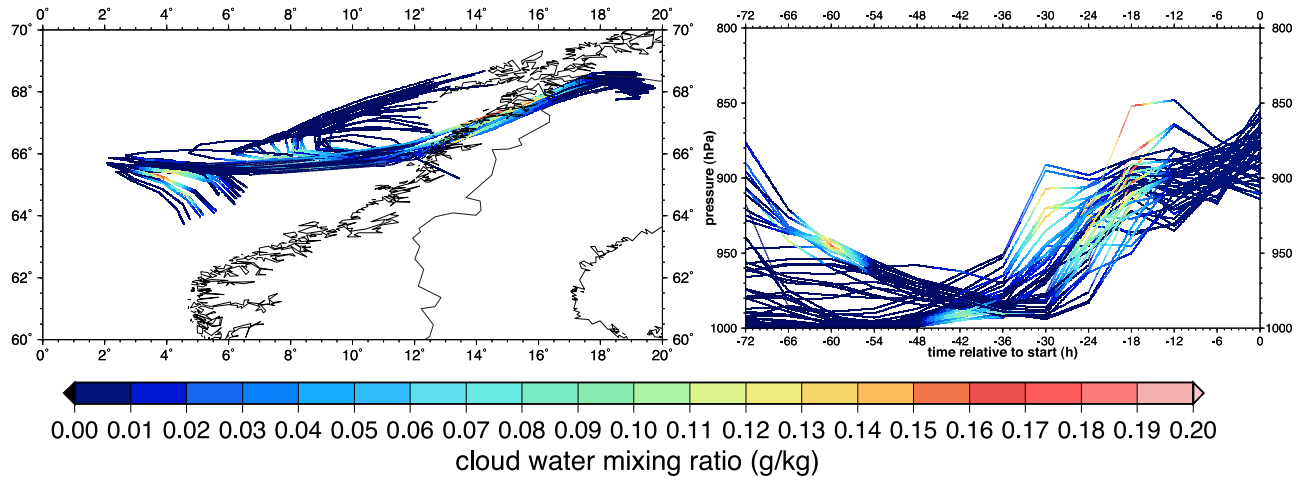

Figure 7. The 72-h trajectories starting 15 July 2007, 0000 UTC, in the region 18.5°E–19.0°E, 68.0°N–68.5°N near ground level (p = 920–850 hPa). (left) Horizontal position of the air parcel. (right) Vertical position of the air parcel. The colors indicate the cloud water mixing ratio which can be interpreted as a cloud proxy.

1.4 and 1.5. A few additional particles with intermediate GFs were detected when DMA2 was periodically deployed in scanning mode although all particles were sorted into the six main bins. In total, 90 bipolar single particle mass spectra from air mass W were sampled. The mass spectra could be sorted into four particle categories: sea salt, potassium-rich, carbon containing, and a group of particles containing several refractory peaks often internally mixed with elemental or organic carbon and sulfates. The majority of particles could be assigned to the last three groups.

[39] The few sea salt particles that were detected had mass spectra with similar peak patterns as described in section 3.1. The mass spectra always contained nitrate peaks while there were minimal chlorine-related peaks if they were present. Thus, these particles can be described as aged sea salt. The second category of particles in the air mass from the W was defined as potassium-rich particles, likely of biomass burning origin (referred to as biomass combustion), as defined in section 3.1. Particles contained carbon-related peaks with the potassium and, very often, sulfate peaks. The remaining aerosol could be roughly defined as carbon containing particles which were subdivided on the basis of refractory material content. The particles from the former group contained mainly EC peaks, often internally mixed with sulfate, and these are likely of combustion origin (these particles are referred to as combustion). The latter particle group also contained metal or mineral dust peaks, often Al^+, V^+, Fe^+, and sometimes Ca^+ or Co^+ (m/z = 59). These particles are referred to as combustion related with metals. In the latter three groups, the fragment peaks of nitrates were often present and/or peaks that could be related to organics (e.g., −26, −42). A total of 9% of the particles did not fit into the four main groups, and these particles are referred to as "others."

[40] The possible sources of the combustion particles are numerous. They may originate from local emissions from the Abisko area or from vehicle traffic. In addition, there are possible aerosol sources from Norway in the west, or the aerosols might have traveled with the air mass for longer times and/or distances. In the two latter cases the combustion particles would have traveled with the air mass over the mountain range without being scavenged in which cases these aerosols were apparently not efficient in forming droplets and did not partition to the cloud phase. It is reasonable to assume that such aerosols would have a

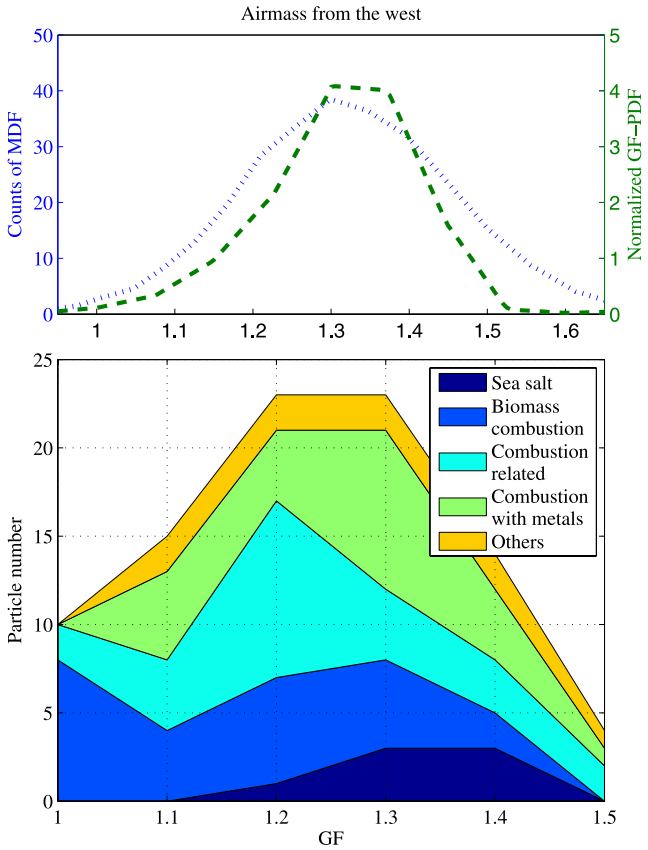

Figure 8. (top) Average of HTDMA scans for the air mass from the west as defined in Figure 3. (bottom) Clustered particle composition and their occurrence as a function of GF for the air mass from the west.

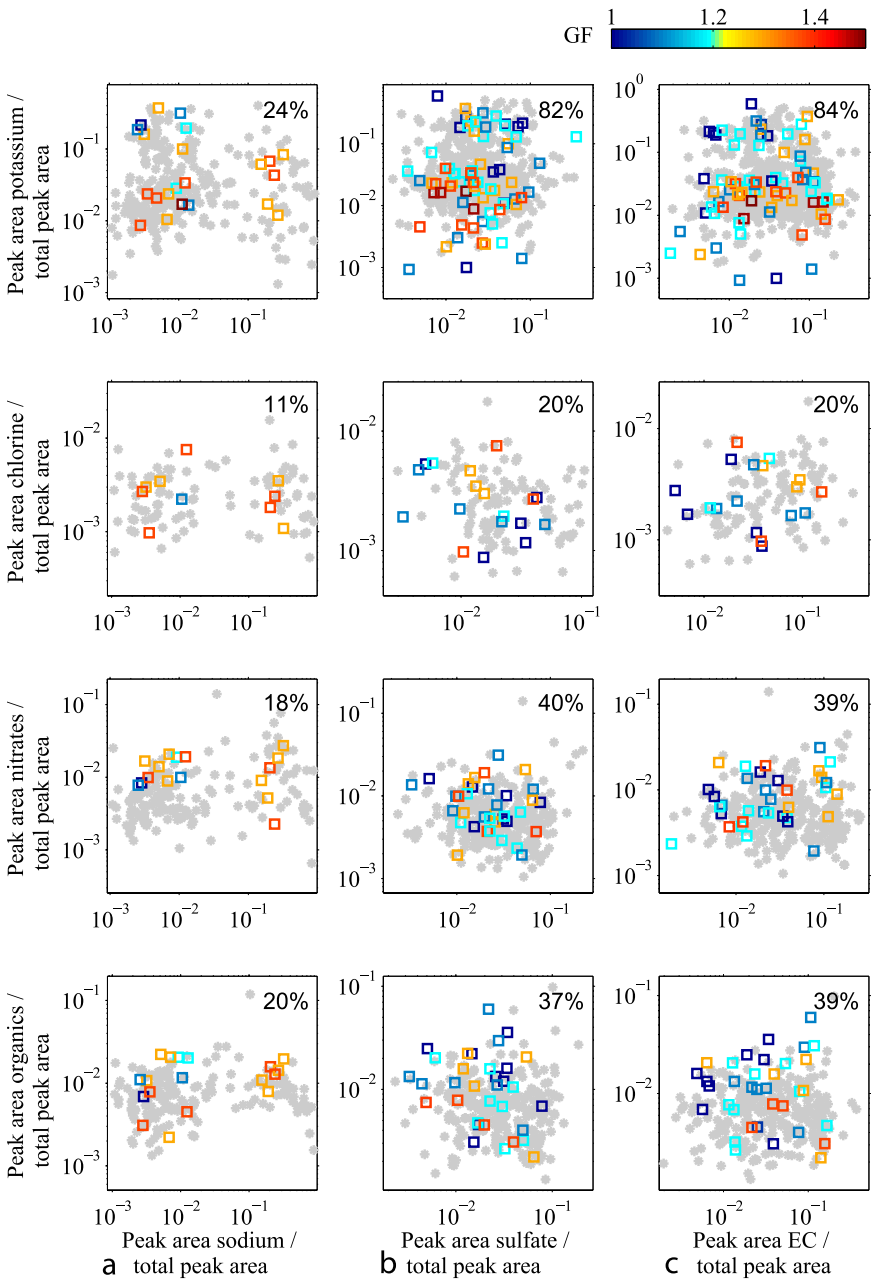

Figure 9. Correlation of different peak area ratios for aerosols from the air mass from the west, analogous to what is shown for the air mass from the northeast in Figure 4. The gray dots indicate the ratios of an ambient sample (766 particles) taken during the same period.

longer atmospheric lifetime and would thus have a relatively larger atmospheric abundance. The 260-nm size lies in the aerosol size range which has a minimum in collection efficiency for scavenging for a typical rain droplet size range, known as the Greenfield gap [*Seinfeld and Pandis*, 2006].

[41] Figure 8 (bottom) shows the distribution of all particles as a function of GF. The sea salt aerosols were found to have GFs of 1.2 and higher. The results for biomass burning related particles were similar to those for the air mass from the NE as these particles were the major source of particles in the nonhygroscopic regime. Specifically, 80% of the particles with a GF of 1.0 originated from this class and this fraction decreased with increasing hygroscopicity. Refractory material containing aerosols were found to have GFs in the range of 1.1 to 1.5 with the highest abundance, 39%, at GF = 1.3. Carbon-rich particles were found over the whole GF range. The highest occurrence was in the mode of GF = 1.2 with a fraction of 43%.

[42] In Figure 9 we show how different peak ratios correlate with each other and the GF, similar to what is shown for the air mass from the NE in Figure 4. For the background, 766 particles from the air mass from the W were sampled between 14 and 18 July. Sea salt was a minor constituent of the aerosols and thus will not be discussed in detail apart from noting that in the first column those

particles with a high relative peak area of sodium have the highest hygroscopicity. Potassium and sodium were present in 24% of the particles where the peak areas of potassium varied between ~0.1 and 50%. As for Figure 4, sea salt related particles are excluded from the second and third columns.

[43] Sulfate and potassium were present in 82% of the particles. Particles with the highest potassium peak area, above 10%, have GF 1.3 and below. More hygroscopic particles, those with GFs of 1.4 and higher, have low potassium peak areas, all below 3%. The sulfate content varied between 0.2 and 30%. Again there is no trend of sulfate peak area and GF as discussed above and by H08. Potassium and EC are found in 91% of the particles with the peak area of potassium varying between ~0.1 and 60%. Again, particles with the highest potassium peak areas have the lowest GFs. The average EC peak area lies between 0.01 and 30% and there is no significant trend with GF. It is noteworthy that the particles with the highest EC peak ratios, above 5%, are only found with a GF of 1.1 or above but none of the GF = 1 particles. As for the air mass from the northeast, this is likely a result of increase signal from potassium at the lowest GFs, not an indication of hygroscopicity being related to EC content. Chlorine was present in 20% of the sulfate/EC particles and there is no apparent relationship between this peak and the GF. Nitrates were present in ~40% of the sulfate/EC particles, which is a higher occurrence when compared to the NE air mass. When present, nitrate peak areas were small, in the range of 0.1–3%. Nitrate peak ratios also did not correlate with GF. Organics were present in 37% and 39% of the sulfate and EC containing particles, respectively. The peak area of organics varied in these particles, in general between 0.2 and 5%, although there was no correlation with GF.

4. Summary

[44] The Arctic is a highly sensitive system with respect to climate change and it has thus become a major research focus in recent years. A better understanding of several processes leading to climate change is still needed and this is one motivation behind the recent International Polar Year (International Council for Science online publication, 2004). One specific point of interest is the limited knowledge of Arctic aerosol particles and their properties relating to, for example, chemistry, visibility, and cloud formation.

[45] The setup of a HTDMA and an ATOFMS connected in series has been shown to be a useful system for determining aerosol chemical composition as a function of hygroscopic growth. During a measurement campaign in the Swedish Arctic two distinct air masses originating from different directions were meteorologically distinguished and particles from each were analyzed. HTDMA scans of D_{dry} = 260 nm aerosols showed a broad monomodal GF distribution centered at ~1.35 (at 82% RH) for both air masses. With the ATOFMS data it was possible to subdivide this peak according to particle composition. In addition, key compounds could be further compared.

[46] For the particles from the NE discrimination was straightforward: most hygroscopic particles were predominantly sea salt. In particular, the sodium peak area of single particle mass spectra correlated strongly with the GF. The nonhygroscopic particles often originated from combustion processes. Particles related to biomass combustion, most likely from local domestic heating, were identified by the indicator potassium and these were found to be the least hygroscopic particle group. This finding was also true for the case of the aerosols sampled in the air mass from the W. These results generally agree with previous work. *Baltensperger et al.* [2002], for example, suggested that nonhygroscopic particles (i.e., GF~1) were fresh emission materials, and *Carrico et al.* [2005] noted that particles containing biomass burning emissions had low hygroscopicity.

[47] Other common aerosol constituents were analyzed as a function of aerosol category and GF. Organics were common in sea salt aerosols and tended to have higher relative peak ratios in these particles than in other classes. For sea salt particles there was no correlation between the organic signal and the GF. This is somewhat contrary to a recent study of sea salt aerosol in a different region [*Facchini et al.*, 2008] and may indicate that the role of organics in sea salt hygroscopicity is more complex than previously thought. Furthermore, there was no correlation of organics with the marker peak Na_2Cl^+, which is related to salt aging, but there was a slight correlation between the Na_2Cl^+ peak and the GF of the salt particles. This is consistent with aged sea salt aerosol being slightly less hygroscopic than newly formed particles. The results for the sea salt aerosols relies on a small data set from one location and during a single season and it would be desirable to increase the number of samples in the future, to cover a broader initial size range, and to collect samples over a longer time period.

[48] The analysis of nitrates showed that these compounds were of low abundance. The exception was in sea salt particles where nitrates had high relative peak areas and thus correlated with hygroscopic growth. It should be stressed that this is a result of the local correlation with sea salt and not a global behavior. For example, H08 found nitrates in a remote continental location correlated with nonhygroscopic mineral dust aerosol, most likely owing to preferential uptake of gas-phase nitric acid [*Henning et al.*, 2003; *Laskin et al.*, 2005]. Sulfates were found in both combustion and sea salt particles and this species, and its relative peak area, was uncorrelated with growth factor. This unexpected behavior, given that sulfate is normally considered hygroscopic, was also observed and discussed by H08 for urban and remote air masses.

[49] Whereas the NE air mass contained a large fraction of sea salt aerosols, the air mass from the W contained only a small fraction despite its maritime origin. Instead, it was shown that most of the particles that reached the sampling site in the W air mass were combustion-related. These findings are likely due to the topography the air masses traveled over. Meteorological records correlated with back trajectories show that when the flow crossed the Scandinavian mountain range it was subject to precipitation and loss of the hygroscopic sea salt. In contrast, the nonhygroscopic combustion aerosols were not subject to wet deposition and remained in the aerosol phase. Thus, in spite of the short distance between the sea and the field site the results show that the lifetime of hygroscopic sea salt aerosols can be very short owing to enhanced washout by orthographic precipitation. The lifetime of combustion particles, likely from

anthropogenic sources, was significantly longer since they were not subject to droplet formation or scavenging.

[50] **Acknowledgments.** This work was supported by ETH internal research funding, the PNNL Aerosol Initiative, and the European Union FP6 infrastructure project EUSAAR (European Supersites for Atmospheric Aerosol Research). We thank the staff at the Abisko Scientific Research Station, as well as Almut Arneth and Thomas Holst and the University of Lund, for support and funding. We also appreciate Markus Gälli for ATOFMS technical support and Andreas Mühlbauer for providing trajectory data.

References

Baltensperger, U., et al. (2002), Urban and rural aerosol characterization of summer smog events during the PIPAPO field campaign in Milan, Italy, *J. Geophys. Res.*, *107*(D22), 8193, doi:10.1029/2001JD001292.

Blanchard, D. (1983), The production, distribution, and bacterial enrichment of the sea-salt aerosol, in *Air-Sea Exchange of Gases and Particles*, edited by P. Liss and W. Slinn, pp. 407–454, D. Reidel, Dordrecht, Netherlands.

Buzorius, G., A. Zelenyuk, F. Brechtel, and D. Imre (2002), Simultaneous determination of individual ambient particle size, hygroscopicity and composition, *Geophys. Res. Lett.*, *29*(20), 1974, doi:10.1029/2001GL014221.

Carrico, C. M., S. M. Kreidenweis, W. C. Malm, D. E. Day, T. Lee, J. Carrillo, G. R. McMeeking, and J. L. Collett (2005), Hygroscopic growth behavior of a carbon-dominated aerosol in Yosemite National Park, *Atmos. Environ.*, *39*(8), 1393–1404, doi:10.1016/j.atmosenv.2004.11.029.

Cavalli, F., et al. (2004), Advances in characterization of size resolved organic matter in marine aerosol in North Atlantic, *J. Geophys. Res.*, *109*, D24215, doi:10.1029/2004JD005137.

Chan, M. N., and C. K. Chan (2005), Mass transfer effects in hygroscopic measurements of aerosol particles, *Atmos. Chem. Phys.*, *5*, 2703–2712.

Charlson, R. J., and M. J. Pilat (1969), Climate: The influence of aerosols, *J. Appl. Meteorol.*, *8*, 1001–1002, doi:10.1175/1520-0450(1969)008<1001:CTIOA>2.0.CO;2.

Cziczo, D. J., D. S. Thomson, and D. M. Murphy (2001), Ablation, flux, and atmospheric implications of meteors inferred from stratospheric aerosol, *Science*, *291*, 1772–1775, doi:10.1126/science.1057737.

Dall'Osto, M., and R. M. Harrison (2006), Chemical characterisation of single airborne particles in Athens (Greece) by ATOFMS, *Atmos. Environ.*, *40*(39), 7614–7631, doi:10.1016/j.atmosenv.2006.06.053.

Dessiaterik, Y., T. Nguyen, T. Baer, and R. E. Miller (2003), IR vaporization mass spectrometry of aerosol particles with ionic solutions: The problem of ion-ion recombination, *J. Phys. Chem. A*, *107*, 11,245–11,252, doi:10.1021/jp036171i.

Dusek, U., et al. (2006), Size matters more than chemistry for cloud-nucleating ability of aerosol particles, *Science*, *312*, 1375–1378, doi:10.1126/science.1125261.

Ehn, M., T. Petäjä, H. Aufmhoff, P. Aalto, K. Hämeri, F. Arnold, A. Laaksonen, and M. Kulmala (2007), Hygroscopic properties of ultrafine aerosol particles in the boreal forest: Diurnal variation, solubility and the influence of sulfuric acid, *Atmos. Chem. Phys.*, *7*, 211–222.

Facchini, M. C., et al. (2008), Primary submicron marine aerosol dominated by insoluble organic colloids and aggregates, *Geophys. Res. Lett.*, *35*, L17814, doi:10.1029/2008GL034210.

Feingold, G., and P. Y. Chuang (2002), Analysis of influence of surface films on droplet growth: Implications for cloud microphysical processes and climate, *J. Atmos. Sci.*, *59*, 2006–2018, doi:10.1175/1520-0469(2002)059<2006:AOTIOF>2.0.CO;2.

Franke, K., A. Ansmann, D. Müller, D. Althausen, C. Venkataraman, M. S. Reddy, F. Wagner, and R. Scheele (2003), Optical properties of the Indo-Asian haze layer over the tropical Indian Ocean, *J. Geophys. Res.*, *108*(D2), 4059, doi:10.1029/2002JD002473.

Friedman, B., H. Herich, L. Kammermann, D. S. Gross, A. Arneth, T. Holst, U. Lohmann, and D. J. Cziczo (2009), Subarctic atmospheric aerosol composition: 1. Ambient aerosol characterization, *J. Geophys. Res.*, *114*, D13203, doi:10.1029/2009JD011772.

Gard, E., J. E. Mayer, B. D. Morrical, R. Dienes, D. P. Fergenson, and K. A. Prather (1997), Real-time analysis of individual atmospheric aerosol particles: Design and performance of a portable ATOFMS, *Anal. Chem.*, *69*, 4083–4091, doi:10.1021/ac970540n.

Gard, E., et al. (1998), Direct observation of heterogeneous chemistry in the atmosphere, *Science*, *279*, 1184–1187, doi:10.1126/science.279.5354.1184.

Gross, D. S., M. E. Gälli, P. J. Silva, and K. A. Prather (2000), Relative sensitivity factors for alkali metal and ammonium cations in single-particle aerosol time-of-flight mass spectra, *Anal. Chem.*, *72*, 416–422, doi:10.1021/ac990434g.

Gysel, M., G. B. McFiggans, and H. Coe (2009), Inversion of tandem differential mobility analyser (TDMA) measurements, *J. Aerosol Sci.*, *40*, 134–151, doi:10.1016/j.jaerosci.2008.07.013.

Hämeri, K., M. Väkevä, P. P. Aalto, M. Kulmala, E. Swietlicki, J. Zhou, W. Seidl, E. Becker, and C. O'Dowd (2001), Hygroscopic and CCN properties of aerosol particles in boreal forests, *Tellus, Ser. B*, *53*, 359–379.

Hatakka, J., et al. (2003), Overview of the atmospheric research activities and results at Pallas GAW station, *Boreal Environ. Res.*, *8*(4), 365–384.

Hegg, D. A., D. S. Covert, K. K. Crahan, H. H. Jonsson, and Y. Liu (2006), Measurements of aerosol size-resolved hygroscopicity at sub and supermicron sizes, *Geophys. Res. Lett.*, *33*, L21808, doi:10.1029/2006GL026747.

Henning, S., E. Weingartner, M. Schwikowski, H. W. Gäggeler, R. Gehrig, K.-P. Hinz, A. Trimborn, B. Spengler, and U. Baltensperger (2003), Seasonal variation of water-soluble ions of the aerosol at the high-alpine site Jungfraujoch (3580 m asl), *J. Geophys. Res.*, *108*(D1), 4030, doi:10.1029/2002JD002439.

Herich, H., L. Kammermann, M. Gysel, E. Weingartner, U. Baltensperger, U. Lohmann, and D. J. Cziczo (2008), In situ determination of atmospheric aerosol composition as a function of hygroscopic growth, *J. Geophys. Res.*, *113*, D16213, doi:10.1029/2008JD009954.

Holecek, J. C., M. T. Spencer, and K. A. Prather (2007), Analysis of rainwater samples: Comparison of single particle residues with ambient particle chemistry from the northeast Pacific and Indian oceans, *J. Geophys. Res.*, *112*, D22S24, doi:10.1029/2006JD008269.

Hu, J. H., and J. P. D. Abbatt (1997), Reaction probabilities for N_2O_5 hydrolysis on sulfuric acid and ammonium sulfate aerosols at room temperature, *J. Phys. Chem.*, *101*, 871–878, doi:10.1021/jp9627436.

Hudson, P. K., D. M. Murphy, D. J. Cziczo, D. S. Thomson, J. A. de Gouw, C. Warneke, J. Holloway, H.-J. Jost, and G. Hübler (2004), Biomass burning particle measurements: Characteristic composition and chemical processing, *J. Geophys. Res.*, *109*, D23S27, doi:10.1029/2003JD004398.

Intergovernmental Panel on Climate Change (IPCC) (2007), *Climate Change 2007: The Physical Science Basis, Contribution of Working Group I to the Fourth Assessment Report of the Intergovernmental Panel on Climate Change*, Cambridge Univ. Press, Cambridge, U. K.

Iversen, T., and E. Joranger (1985), Arctic air pollution and large scale atmospheric flows, *Atmos. Environ.*, *19*(12), 2099–2108, doi:10.1016/0004-6981(85)90117-9.

Klonecki, A., P. Hess, L. Emmons, L. Smith, J. Orlando, and D. Blake (2003), Seasonal changes in the transport of pollutants into the Arctic troposphere-model study, *J. Geophys. Res.*, *108*(D4), 8367, doi:10.1029/2002JD002199.

Koehler, K. A., S. M. Kreidenweis, P. J. DeMott, A. J. Prenni, C. M. Carrico, B. Ervens, and G. Feingold (2005), Water activity and activation diameters from hygroscopicity data. Part II: Application to organic species, *Atmos. Chem. Phys.*, *6*, 795–809.

Kreidenweis, S. M., K. Koehler, P. J. DeMott, A. J. Prenni, C. Carrico, and B. Ervens (2005), Water activity and activation diameters from hygroscopicity data. Part I: Theory and application to inorganic salts, *Atmos. Chem. Phys.*, *5*, 1357–1370.

Kulmala, M., et al. (2001), Overview of the international project on biogenic aerosol formation in the boreal forest (BIOFOR), *Tellus, Ser. B*, *53*, 324–343, doi:10.1034/j.1600-0889.2001.d01-24.x.

Laskin, A., T. W. Wietsma, B. J. Krueger, and V. H. Grassian (2005), Heterogeneous chemistry of individual mineral dust particles with nitric acid: A combined CCSEM/EDX, ESEM, and ICP-MS study, *J. Geophys. Res.*, *110*, D10208, doi:10.1029/2004JD005206.

Leck, C., and E. K. Bigg (1999), Aerosol production over remote marine areas—A new route, *Geophys. Res. Lett.*, *26*(23), 3577–3580, doi:10.1029/1999GL010807.

Leck, C., M. Norman, E. K. Bigg, and R. Hillamo (2002), Chemical composition and sources of the high Arctic aerosol relevant for cloud formation, *J. Geophys. Res.*, *107*(D12), 4135, doi:10.1029/2001JD001463.

Liu, B. Y. H., D. Y. H. Pui, K. T. Whitby, D. B. Kittelson, Y. Kousaka, and R. L. McKenzie (1978), Aerosol mobility chromatograph—New detector for sulfuric-acid aerosols, *Atmos. Environ.*, *12*(1–3), 99–104, doi:10.1016/0004-6981(78)90192-0.

Liu, P., P. J. Ziemann, D. B. Kittelson, and P. H. McMurry (1995a), Generating particle beams of controlled dimensions and divergence: I. Theory of particle motion in aerodynamic lenses and nozzle expansions, *Aerosol Sci. Technol.*, *22*, 293–313, doi:10.1080/02786829408959748.

Liu, P., P. J. Ziemann, D. B. Kittelson, and P. H. McMurry (1995b), Generating particle beams of controlled dimensions and divergence: II. Experimental evaluation of particle motion in aerodynamic lenses and

nozzle expansions, *Aerosol Sci. Technol.*, *22*, 314–324, doi:10.1080/02786829408959749.
Lohmann, U., and J. Feichter (2005), Global indirect aerosol effects: A review, *Atmos. Chem. Phys.*, *5*, 715–737.
Lohmann, U., and C. Leck (2005), Importance of submicron surface-active organic aerosols for pristine Arctic clouds, *Tellus, Ser. B*, *57*, 261–268, doi:10.1111/j.1600-0889.2005.00144.x.
Malm, W. C., D. E. Day, S. M. Kreidenweis, J. L. Collett, and T. Lee (2003), Humidity-dependent optical properties of fine particles during the Big Bend Regional Aerosol and Visibility Observational Study, *J. Geophys. Res.*, *108*(D9), 4279, doi:10.1029/2002JD002998.
Marcolli, C., B. P. Luo, and T. Peter (2004), Mixing of the organic aerosol fractions: Liquids as the thermodynamically stable phases, *J. Phys. Chem.*, *108*, 2216–2224.
McCormick, R. A., and J. H. Ludwig (1967), Climate modification by atmospheric aerosols, *Science*, *156*, 1358–1359, doi:10.1126/science.156.3780.1358.
McMurry, P. H., M. Litchy, P. F. Huang, X. Cai, B. Turpin, W. D. Dick, and A. Hanson (1996), Elemental composition and morphology of individual particles separated by size and hygroscopicity with the TDMA, *Atmos. Environ.*, *30*(1), 101–108, doi:10.1016/1352-2310(95)00235-Q.
Middlebrook, A. M., D. M. Murphy, and D. S. Thomson (1998), Observations of organic material in individual marine particles at Cape Grim during the first Aerosol Characterization Experiment (ACE 1), *J. Geophys. Res.*, *103*(D13), 16,475–16,483, doi:10.1029/97JD03719.
Middlebrook, A. M., et al. (2003), A comparison of particle mass spectrometers during the 1999 Atlanta Supersite Project, *J. Geophys. Res.*, *108*(D7), 8424, doi:10.1029/2001JD000660.
Ming, Y., and L. M. Russell (2001), Predicted hygroscopic growth of sea salt aerosol, *J. Geophys. Res.*, *106*(D22), 28,259–28,274, doi:10.1029/2001JD000454.
Mozurkewich, M., and J. G. Calvert (1988), Reaction probability of N_2O_5 on aqueous aerosols, *J. Geophys. Res.*, *93*(D12), 15,889–15,896, doi:10.1029/JD093iD12p15889.
Murphy, D. M. (2007), The design of single particle laser mass spectrometers, *Mass Spectrom. Rev.*, *26*, 150–165, doi:10.1002/mas.20113.
Murphy, D. M., and D. S. Thomson (1997a), Chemical composition of single aerosol particles at Idaho Hill: Negative ion measurements, *J. Geophys. Res.*, *102*(D5), 6353–6368, doi:10.1029/96JD00859.
Murphy, D. M., and D. S. Thomson (1997b), Chemical composition of single aerosol particles at Idaho Hill: Positive ion measurements, *J. Geophys. Res.*, *102*(D5), 6341–6352, doi:10.1029/96JD00858.
Murphy, D. M., D. J. Cziczo, K. D. Froyd, P. K. Hudson, B. M. Matthew, A. M. Middlebrook, R. E. Peltier, A. Sullivan, D. S. Thomson, and R. J. Weber (2006), Single-particle mass spectrometry of tropospheric aerosol particles, *J. Geophys. Res.*, *111*, D23S32, doi:10.1029/2006JD007340.
O'Dowd, C. D., P. Aalto, K. Hämeri, M. Kulmala, and T. Hoffmann (2002), Aerosol formation: Atmospheric particles from organic vapours, *Nature*, *416*, 497–498, doi:10.1038/416497a.
O'Dowd, C. D., M. C. Facchini, F. Cavalli, D. Ceburnis, M. Mircea, S. Decesari, S. Fuzzi, Y. J. Yoon, and J.-P. Putaud (2004), Biogenically driven organic contribution to marine aerosol, *Nature*, *431*, 676–680, doi:10.1038/nature02959.
Pitchford, M., and P. McMurry (1994), Relationship between measured water vapor growth and chemistry of atmospheric aerosol for Grand Canyon, Arizona, in winter 1990, *Atmos. Environ.*, *28*(5), 827–840, doi:10.1016/1352-2310(94)90242-9.
Quinn, P. K., et al. (2008), Short-lived pollutants in the Arctic: Their climate impact and possible mitigation strategies, *Atmos. Chem. Phys.*, *8*, 1723–1735.
Randles, C. A., L. M. Russell, and V. Ramaswamy (2004), Hygroscopic and optical properties of organic sea salt aerosol and consequences for climate forcing, *Geophys. Res. Lett.*, *31*, L16108, doi:10.1029/2004GL020628.
Rosenfeld, D., and I. M. Lensky (1998), Satellite-based insights into precipitation formation processes in continental and maritime convective clouds, *Bull. Am. Meteorol. Soc.*, *79*, 2457–2476, doi:10.1175/1520-0477(1998)079<2457:SBIIPF>2.0.CO;2.
Satheesh, S. K., and V. Ramanathan (2000), Large difference in tropical aerosol forcing at the top of the atmosphere and Earth's surface, *Nature*, *405*, 60–63, doi:10.1038/35011039.
Saxena, P., L. M. Hildemann, P. H. McMurry, and J. H. Seinfeld (1995), Organics alter hygroscopic behavior of atmospheric particles, *J. Geophys. Res.*, *100*(D9), 18,755–18,770, doi:10.1029/95JD01835.
Schmid, H., et al. (2001), Results of the "carbon conference" international aerosol carbon round robin test stage I, *Atmos. Environ.*, *35*(12), 2111–2121, doi:10.1016/S1352-2310(00)00493-3.
Schwartz, S. E. (1996), The whitehouse effect—Shortwave radiative forcing of climate by anthropogenic aerosols: An overview, *J. Aerosol Sci.*, *27*, 359–382, doi:10.1016/0021-8502(95)00533-1.
Seinfeld, J. H., and S. N. Pandis (2006), *Atmospheric Chemistry and Physics*, John Wiley, Hoboken, N. J.
Silva, P. J., D.-Y. Liu, C. A. Noble, and K. A. Prather (1999), Size and chemical characterization of individual particles resulting from biomass burning of local Southern California species, *Environ. Sci. Technol.*, *33*(18), 3068–3076, doi:10.1021/es980544p.
Sjogren, S., M. Gysel, E. Weingartner, U. Baltensperger, M. J. Cubison, H. Coe, A. Zardini, C. Marcolli, U. K. Krieger, and T. Peter (2007), Hygroscopic growth and water uptake kinetics of two-phase aerosol particles consisting of ammonium sulfate, adipic and humic acid mixtures, *J. Aerosol Sci.*, *38*, 157–171, doi:10.1016/j.jaerosci.2006.11.005.
Sohlenius, B., and S. Boström (1999), Effects of climate change on soil factors and metazoan microfauna (nematodes, tardigrades and rotifers) in a Swedish tundra soil—A soil transplantation experiment, *Appl. Soil Ecol.*, *12*, 113–128, doi:10.1016/S0929-1393(98)00168-1.
Sonesson, M. (1980), Ecology of a subarctic mire, *Ecol. Bull.*, *30*, 313–323.
Svenningsson, B., et al. (2006), Hygroscopic growth and critical supersaturations for mixed aerosol particles of inorganic and organic compounds of atmospheric relevance, *Atmos. Chem. Phys.*, *6*, 1937–1952.
Svenningsson, B., et al. (2008), Aerosol particle formation events and analysis of high growth rates observed above a subarctic wetland forest mosaic, *Tellus, Ser. B*, *60*, 353–364.
Swietlicki, E., et al. (2008), Hygroscopic properties of sub-micrometer atmospheric aerosol particles measured with H-TDMA instruments in various environments—A review, *Tellus, Ser. B*, *60*, 432–469, doi:10.1111/j.1600-0889.2008.00350.x.
Twomey, S. (1977), The influence of pollution on the shortwave albedo of clouds, *J. Atmos. Sci.*, *34*, 1149–1152, doi:10.1175/1520-0469(1977)034<1149:TIOPOT>2.0.CO;2.
Weingartner, E., S. Nyeki, and U. Baltensperger (1999), Seasonal and diurnal variation of aerosol size distributions ($10 < D < 750$ nm) at a high-alpine site (Jungfraujoch 3580 m asl), *J. Geophys. Res.*, *104*(D21), 26,809–26,820, doi:10.1029/1999JD900170.
Weingartner, E., M. Gysel, and U. Baltensperger (2002), Hygroscopicity of aerosol particles at low temperatures. 1. New low-temperature H-TDMA instrument: Setup and first applications, *Environ. Sci. Technol.*, *36*, 55–62, doi:10.1021/es010054o.
Weiss, M., P. J. T. Verheijen, J. C. M. Marijnissen, and B. Scarlett (1997), On the performance of an on-line time-of-flight mass spectrometer for aerosols, *J. Aerosol Sci.*, *28*, 159–171, doi:10.1016/S0021-8502(96)00067-5.
Wenzel, R. J., D.-Y. Liu, E. S. Edgerton, and K. A. Prather (2003), Aerosol time-of-flight mass spectrometry during the Atlanta Supersite Experiment: 2. Scaling procedures, *J. Geophys. Res.*, *108*(D7), 8427, doi:10.1029/2001JD001563.
Wernli, H., and H. C. Davies (1997), A Lagrangian-based analysis of extratropical cyclones. I: The method and some applications, *Q. J. R. Meteorol. Soc.*, *123*, 467–489, doi:10.1002/qj.49712353811.
Yu, H., et al. (2006), A review of measurement-based assessment of aerosol direct radiative effect and forcing, *Atmos. Chem. Phys.*, *6*, 613–666.
Zelenyuk, A., D. Imre, J. Han, and S. Oatis (2008), Simultaneous measurements of individual ambient particles size, composition, effective density, and hygroscopicity, *Anal. Chem.*, *80*, 1401–1407, doi:10.1021/ac701723v.

U. Baltensperger, M. Gysel, L. Kammermann, and E. Weingartner, Laboratory of Atmospheric Chemistry, Paul Scherrer Institut, CH-5232 Villigen, Switzerland.

D. J. Cziczo, Atmospheric Science and Global Change, Pacific Northwest National Laboratory, 3200 Q Avenue, Richland, WA 99352, USA. (Daniel.cziczo@pnl.gov)

B. Friedman, Department of Atmospheric Sciences, University of Washington, Seattle, WA 98195, USA.

D. S. Gross, Department of Chemistry, Carleton College, 1 North College Street, Northfield, MN 55057, USA.

H. Herich, U. Lohmann, and P. Spichtinger, Institute for Atmospheric and Climate Science, ETH Zurich, CH-8092 Zurich, Switzerland.